# Competition between Dukhin's and Rubinstein's electrokinetic modes

H.-C. Chang,[1] E. A. Demekhin,[2,3] and V. S. Shelistov[2]

[1]*Department of Chemical and Biomolecular Engineering, Center for Microfluidics and Medical Diagnostics, University of Notre Dame, Notre Dame, Indiana 46556, USA*

[2]*Department of Computation Mathematics and Computer Science, Kuban State University, Krasnodar 350040, Russian Federation*

[3]*Laboratory of Micro- and Nanofluidics, Department of Physics of Polymers and Crystals, Faculty of Physics, Moscow State University, Moscow, 119991, Russian Federation*

The combined effect of two modes of electroconvection, i.e., (a) the electro-osmotic flow of the second kind induced by a curved membrane surface and (b) electrokinetic instability, is studied numerically. Both physical mechanisms are responsible for electric current enhancement to the surface, and these modes are strongly nonlinearly coupled. For the limiting regimes, their resonant interaction near the threshold of instability with a corresponding resonantly amplified current enhancement is found. For the overlimiting regimes, inside the unstable region, their interaction becomes more complex with negative "sideband" and positive "subharmonic" resonant interactions. Wall corrugation can still be in resonance with the unstable modes. At some wave numbers of corrugation, these two mechanisms compete and electrokinetic instability can even be completely suppressed by the wall corrugation.

## I. INTRODUCTION

Extended polarization near a charge-selective surface (a membrane, electrode, or system of micro- or nanochannels) can drive a hydrodynamic flow if a tangential electric field exists and, hence, the local velocity is a product of the normal and tangential components of the electric field. In particular, (a) a surface with curvature can be responsible for the existence of both field components (so-called Dukhin's mechanism [1]) and (b) the extended polarization layer near a flat charge-selective surface can be unstable to small perturbations (electroconvective or electrokinetic instability, which theory was first advanced by Rubinstein and Zaltzman [2]). There is also bulk electroconvective instability, which pertains to the flow induced by the action of the mean electric field upon the residual space charge in the macroscopic regions of a locally quasielectroneutral strong electrolyte; see [3], and the references therein.

It is obvious that a geometrical surface inhomogeneity can essentially influence electroconvective instability and cause electric current enhancement to the surface. Rubinstein and Zaltzman's [2] estimation for a model system of equations is that a 10% distortion of the flat surface results in a 30% enhancement in the current to the surface.

In this paper, we present a numerical study of the full Nernst-Planck-Poisson-Stokes system in the region between flat and corrugated membranes under a fixed potential drop. The dependence of the ion flux on the wave number of corrugation $q$ and its amplitude $a$ has been investigated for the limiting and overlimiting regimes. Subject to the system parameters, two modes of electroconvection can either weaken or amplify the electric current enhancement to the surface.

## II. FORMULATION

A symmetric, binary electrolyte with an equal diffusivity of cations and anions $\tilde{D}$, dynamic viscosity $\tilde{\mu}$, and permittivity $\tilde{d}$ is considered. The two-dimensional solution between an upper, ideal semiselective ion-exchange membrane at $\tilde{y} = \tilde{L}$ and a corrugated lower membrane at $\tilde{y} = \tilde{h}(\tilde{x})$ is studied. Notations

with tildes are used for the dimensional variables, as opposed to their dimensionless counterparts without tildes; $\{\tilde{x}, \tilde{y}\}$ are the coordinates, where $\tilde{x}$ is directed along the upper membrane's surface and $\tilde{y}$ is normal to that surface; and $\{\tilde{U}, \tilde{V}\}$ are the correspondent velocity components.

The flow is assumed to be Stokes creeping flow. Then the system of equations is

$$\nu^2 \nabla^2 \Phi = c^- - c^+ = -\rho, \tag{1}$$

$$\nabla^4 \Psi = \frac{\kappa}{\nu^2} \left[ \frac{\partial}{\partial y} \left( \rho \frac{\partial \Phi}{\partial x} \right) - \frac{\partial}{\partial x} \left( \rho \frac{\partial \Phi}{\partial y} \right) \right], \tag{2}$$

$$\frac{\partial c^\pm}{\partial t} + \mathbf{U} \cdot \nabla c^\pm = \pm \nabla \cdot (c^\pm \nabla \Phi) + \nabla^2 c^\pm. \tag{3}$$

Here, $\mathbf{U} = (\partial \Psi / \partial y, -\partial \Psi / \partial x)$ is the velocity vector. The system is taken in a dimensionless form with $\tilde{L}$ as the characteristic length, $\tilde{L}^2 / \tilde{D}$ as the characteristic time, and $\tilde{\mu}$ as the dynamical characteristic value; the potential $\tilde{\Phi}_0 = \tilde{R}\tilde{T}/\tilde{F}$ is taken as the characteristic potential, the bulk concentration of the electroneutral solution is $t = 0$, and $\tilde{c}_0$ is the characteristic concentration. The parameter $\kappa = \tilde{d}\tilde{\Phi}_0^2 / \tilde{\mu}\tilde{D}$ appears as a coupling coefficient between the hydrodynamics and the electrostatics. It is essential that the coupling coefficient depends only upon the physical properties of the electrolyte. $\nu$ is the dimensionless Debye length, $\nu = \tilde{\lambda}_D / \tilde{L}$ and $\tilde{\lambda}_D = \sqrt{\tilde{d}\tilde{\Phi}_0 / \tilde{F}\tilde{c}_0}$, $\tilde{R}$ is the universal gas constant, $\tilde{T}$ is the absolute temperature, and $\tilde{F}$ is the Faraday constant.

The boundary conditions at the membrane surfaces are

$$y = h(x): c^+ = p, \quad -c^- \frac{\partial \Phi}{\partial n} + \frac{\partial c^-}{\partial n} = 0,$$
$$U = V = 0, \quad \Phi = 0, \tag{4}$$

$$y = 1: c^+ = p, \quad -c^- \frac{\partial \Phi}{\partial y} + \frac{\partial c^-}{\partial y} = 0,$$
$$U = V = 0, \quad \Phi = \Delta V, \tag{5}$$

where the normal vector $n$ is directed from the surface into the liquid. The first pair of conditions, prescribing an interface

concentration equal to that of the fixed charges inside the membrane, is asymptotically valid for large $p$ and was first introduced by Rubinstein (see, for example, [4,5], and the references therein). These conditions, prescribing an interface concentration equal to that of the fixed charges inside the membrane, $p$, are asymptotically valid for $p \gg 1$ and amount to disregarding the co-ion invasion of an ideally semiselective membrane. Hence, the second pair of conditions means that the membrane is ideally permselective, and, thus, there is no anion flux. The third pair is the usual no-slip condition, and the last one fixes the potential at the lower membrane's surface to be zero and specifies the potential drop across the membranes.

The density of the electric current through the curved surface $y = h(x)$ is determined by

$$j = \frac{1}{4}\left(c^{+}\frac{\partial \Phi}{\partial n} + \frac{\partial c^{+}}{\partial n}\right), \tag{6}$$

with

$$\frac{\partial}{\partial n} = \frac{\partial x}{\partial n}\frac{\partial}{\partial x} + \frac{\partial y}{\partial n}\frac{\partial}{\partial y} = -\frac{h_x}{\sqrt{1+h_x^2}}\frac{\partial}{\partial x} + \frac{1}{\sqrt{1+h_x^2}}\frac{\partial}{\partial y},$$

$$h_x \equiv \frac{\partial h}{\partial x}. \tag{7}$$

Taking into account that $\Phi = \text{const}$ along $y = h(x)$, the second boundary condition (4) turns into

$$-c^{-}\frac{\partial \Phi}{\partial y} + \frac{\partial c^{-}}{\partial y} - h_x\frac{\partial c^{-}}{\partial x} = 0. \tag{8}$$

For the current density $j$, the fact that $c^{+} = \text{const}$ along the membrane is utilized:

$$j = \frac{1}{4}\left(c^{+}\frac{\partial \Phi}{\partial y} + \frac{\partial c^{+}}{\partial y}\right) \Big/ \sqrt{1+h_x^2}. \tag{9}$$

A periodicity with period $q$ in the $x$ coordinate is assumed, and most of the calculations were done for simple sinusoidal perturbations,

$$y = h(x) = a\cos qx. \tag{10}$$

It is convenient to describe the final solution, as $t \to \infty$, by averaging over the period of corrugation, $2\pi/q$, electric current $\langle j \rangle$, and amplitude of the electric current $j_{\max} - j_{\min}$, as follows:

$$\langle j \rangle = \frac{1}{l}\int_0^l j(x)\,dl = \frac{q}{2\pi}\int_0^{2\pi/q} j(x)\sqrt{1+h_x^2}\,dx,$$

$$j_{\max} - j_{\min} = \max_{0<x<l} j(x) - \min_{0<x<l} j(x) \text{ at } t \to \infty. \tag{11}$$

The geometry is shown in Fig. 1.

The problem is described by five dimensionless parameters: the potential drop $\Delta V$, the Debye number $\nu$, which is a small parameter of the system, the coupling coefficient between the electrostatics and the hydrodynamics $\kappa$, the wave number of corrugation $q$, and its amplitude $a$. The dependence on the concentration $p$ for the overlimiting regimes is practically absent, so $p$ is not included in the parameters mentioned.

## III. NUMERICAL SOLUTION

The direct numerical simulation of the system (1)–(10), without any simplification, is implemented by applying the
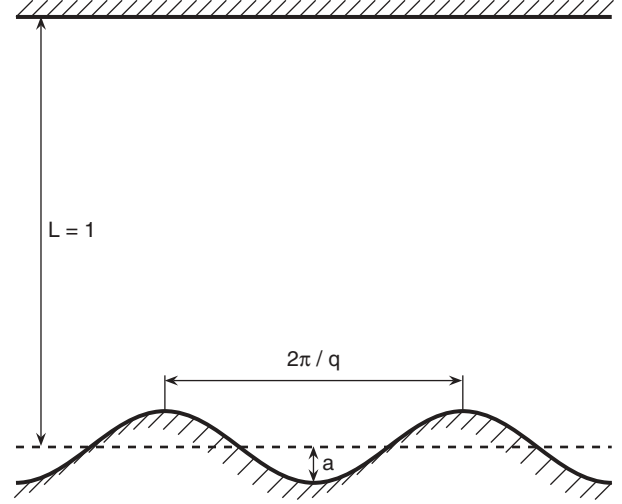


FIG. 1. Geometry of the flow: the upper flat and lower curved surfaces are ideally permselective membranes with a potential drop $\Delta V$ between them. The extended space charge (ESC) region is located near the lower membrane

Galerkin pseudospectral $\tau$ method. A periodic domain along the membrane surface allows the utilization of a Fourier series, $\exp(inkx)$, in the $x$ direction. Chebyshev polynomials $T_m(y)$ are used in the transverse direction $y$. Eventually, the physical variables take the form

$$\Phi = \sum_{m=0}^{M}\sum_{n=-N}^{N}\Phi_{mn}e^{inkx}T_m(y),$$

$$\Psi = \sum_{m=0}^{M}\sum_{n=-N}^{N}\Psi_{mn}e^{inkx}T_m(y), \quad c^{\pm} = \sum_{m=0}^{M}\sum_{n=-N}^{N}c_{mn}^{\pm}e^{inkx}T_m(y).$$

The reality of the solutions implies $\Phi_{m,-n} = \bar{\Phi}_{m,n}$, $\Psi_{m,-n} = \bar{\Psi}_{m,n}$, and $c_{m,-n}^{\pm} = \bar{c}_{m,n}^{\pm}$, where the barred quantities are complex conjugates. The basic wave number $k$ characterizes the length of the considered domain, $2\pi/k$, while $q$ characterizes the "density" of the corrugation. The main difficulty in dealing with the electrokinetic instability is to resolve the structure of the unknowns close to the electrodes [5]. The accumulation of zeros of the Chebyshev polynomials near the walls, along with the fact that there are rather a large number of them, allows properly resolving the thin space charge regions. The number of Fourier modes and Chebyshev polynomials were taken, respectively, to be $N = 64$–256 and $M = 128$–512; the accuracy of the calculations and the convergence of the code were monitored by changing $N$ and $M$. The Chebyshev grid enabled us to concentrate the grid points near the boundary layers, although not in an optimal way.

The numerical solution of Eqs. (1)–(3) in a complex domain with the conditions (4) at the boundary of this domain can be obtained by using (a) boundary-fitted grids or (b) the immersed-boundary method and performing a simulation in simple rectangular domains, which contain the original domain with a complex geometry. There are many different variations of the immersed-boundary method. In the present paper, some ideas of [6–8] for the Navier-Stokes system are adapted for our Nernst-Planck-Poisson-Stokes system, given by Eqs. (3)–(10).

The fundamental idea is to transform the domain into a rectangular one, such that the lower artificial boundary $y = h_{\min}$ is flat instead of wavy, as was the original boundary $h(x)$. To impose the conditions (4) on the wavy boundary, source terms for $\Phi$, $\Psi$, $c^+$, and $c^-$ are added to the governing equations (1)–(3). The purpose of these terms is to impose the boundary conditions (4) on the immersed boundary $y = h(x)$. The main advantage of this method is that it is based on the same numerical codes as those used in [9] for a rectangular region. The main disadvantage, however, is the difficulty in resolving the local double-ion layer and extended space charge regions near the corrugated wall with sharp variations of the unknowns. These are especially pronounced for the limiting and overlimiting regimes.

Let us enumerate the basic ideas and steps of this method. Inside our calculations, we stretched the variables $x$ and $y$ in such a way that the flat artificial boundary was located at $y = 0$ and the upper one was located at $y = 1$. For our eventual presentation of the results, we returned to the previous independent variables.

Substituting the finite Fourier-Chebyshev series into the governing system and using the Lanczos procedure along with the artificial source terms to satisfy the boundary conditions led to a system of coupled ordinary differential equations for the unknown Galerkin coefficients. To obtain these equations, all nonlinear algebraic operations were executed in physical space, at the collocation points, while the derivatives with respect to both spatial variables $x$ and $y$ were calculated in the space of the Galerkin coefficients. The derivatives of the Chebyshev polynomials were calculated by means of the collocation matrix method (see [10]). The connection between the collocation points and the Galerkin coefficients is performed by means of the fast discrete cosine transform.

(1) With the charge density $\rho$ from the previous time step $t$, we can find the solution $\Phi$ of the boundary problem for the Poisson equation as follows.

(1.1) Let us present $\Phi$ as a superposition, $\Phi = F + \hat{\Phi}$, where $F$ obeys the equations in the rectangular region

$$\frac{\partial^2 F}{\partial x^2} + \frac{\partial^2 F}{\partial y^2} = -\frac{\rho}{\nu^2}, \quad F(0) = 0, \quad F(1) = \Delta V, \quad (12)$$

and $\hat{\Phi}$ is the correction term which is related with the source term. The problem for the rectangular region (12) was solved numerically using the Galerkin method [9].

(1.2) In order to find the correction term $\hat{\Phi}$, the following set of subproblems was considered:

$$\frac{\partial^2 \hat{\Phi}_n}{\partial x^2} + \frac{\partial^2 \hat{\Phi}_n}{\partial y^2} = \delta(x - x_n)\delta(y - h_n),$$
$$\hat{\Phi}_n(0) = \hat{\Phi}_n(1) = 0, \quad n = 0, 1, \ldots, N, \quad (13)$$

where $\delta(x)$ and $\delta(y)$ are Dirac delta functions which were taken at the discrete set of points $x_n$ and $h_n = h(x_n)$ at the boundary $y = h(x)$. The problems (13) can be solved either analytically or numerically; we chose a numerical method.

(1.3) Our solution is a superposition

$$\Phi = F + \hat{\Phi} = F + \sum_{n=0}^{N} A_n \hat{\Phi}_n, \quad (14)$$

where $A_n$ are unknown constants, which were found from the requirement that $\Phi$ vanishes at the discrete points of the boundary $y = h(x)$,

$$\sum_{n=0}^{N} A_n \hat{\Phi}_n = -F \text{ at the points } x_n, h_n. \quad (15)$$

The boundary $y = h(x)$ was fixed in time, hence, the matrix of the linear algebraic system (15) was also fixed and can be inverted only once, at the beginning of calculations.

(2) With the charge density $\rho$ and potential $\Phi$ known at the time level $t$, the biharmonic equation (2) is ready to be solved. Because the biharmonic equation can be presented as a system of two Poisson equations, which allows it to be solved by the above-described algorithm, we omit any detailed description of this step.

(3) The Eqs. (3) are nonstationary equations and, hence, their solution is different from that described above. The ideas of [6–8] were employed as follows.

(3.1) As a provisional step to find the solution at the next time level $t + \Delta t$, the equation (3) for positive ions was solved in the rectangular region with the boundary conditions at $y = 0$ and $y = 1$, $c^+ = p$. The time integration was performed explicitly.

(3.2) The solution found was then corrected: $c^+$ was forced to be equal to $c^+ = p$ at the set of points $x = x_n$ and $y = h_n$.

(3.3) An unknown source term $f_{C^+}$ was added to Eq. (3),

$$\frac{\partial c^+}{\partial t} + \mathbf{U} \cdot \nabla c^+ = \nabla \cdot (c^+ \nabla \Phi) + \nabla^2 c^+ + f_{C^+}. \quad (16)$$

The corrected solution is used to find the source term from the equation

$$f_{C^+} = \begin{cases} \{\mathbf{U}\nabla c^+ - \nabla(c^+ \nabla \Phi) - \nabla^2 c^+\} & \text{at the boundary points } x_n, h_n; \\ 0 & \text{at all other points.} \end{cases} \quad (17)$$

Here, it is taken into account that the derivative $\partial c^+/\partial t = 0$ at $y = h(x)$.

(4) The procedure for finding $c^-$ was rather similar to the aforementioned one; it also included the source term $f_{C^-}$, but technically was more complex because the boundary condition

of the first kind was changed to a boundary condition of the third kind (8).

(5) A special semi-implicit method was developed to integrate Eq. (16) in time with the known source terms $f_{C^+}$ and $f_{C^-}$. The ion transport equations for the concentrations
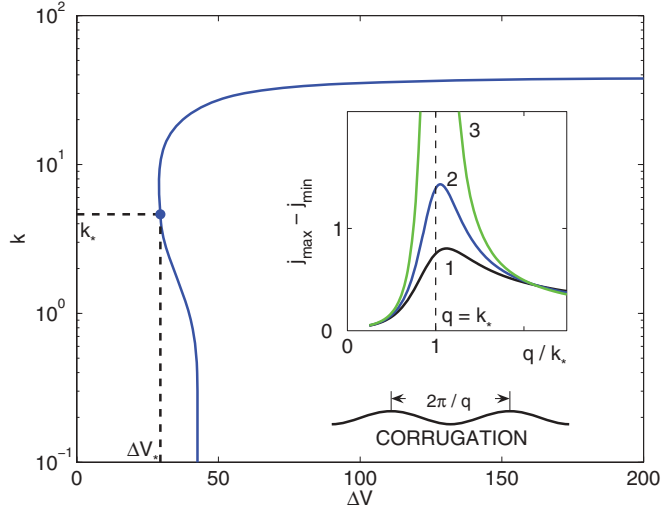
FIG. 2. (Color online) Marginal stability curve for $\nu = 10^{-3}$ and $\kappa = 0.1$ with a critical point at $\Delta V_* = 29.5$ and $k_* = 4.63$. Inset: linear response to the corrugation for different $\Delta V / \Delta V_*$: (1) 0.93, (2) 0.99, and (3) 1.00; this response becomes infinitely large at $q = k_*$ and $\Delta V = \Delta V_*$.

are integrated and $c_{mn}^{\pm}(t + \Delta t)$ are found for the next time level $t + \Delta t$. The second-order Adams-Bashforth scheme for nonlinear terms and the Crank-Nicholson scheme for linear terms were used.

*Comment No. 1.* Since the function $y = h(x)$ does not necessarily coincide with the grid points, the conditions on

the wavy boundary were extended to the grid points by means of biquadratic interpolation.

*Comment No. 2.* Before transforming the functions $\Phi$, $\Psi$, and $c^{\pm}$ to Galerkin space, they were smoothed by multiplying them by a narrow distribution function. This transform was adopted from [6],

$$\Phi_{\text{smooth}} = \sum_{i,j} \Phi(x_i, y_j) e^{-a_x(x-x_i)^2 - a_y(y-y_j)^2},$$

and similarly for the other functions, where $(x_i, y_j)$ were the grid points near the wavy boundary $y = h(x)$, and $a_x$ and $a_y$ were properly chosen numbers. The Galerkin representation of the correction functions was also filtered to suppress the highest modes and thus reduce the unnatural oscillations that arose due to singularities in those functions.

The results of the calculation are presented for the Debye number $\nu = 10^{-3}$ and for a typical value of the coupling coefficient $\kappa = 0.1$; $p = 5$ is kept.

## IV. RESULTS AND DISCUSSION

For the limiting and overlimiting regimes, there is a thin layer of extended space charge (ESC) region $O(\nu^{2/3})$ (see [5]), which behaves like a free surface [9]. If the ESC layer is thinned by a localized perturbation, then the electric field $E$ increases and the electrostatic pressure in the layer increases as $E^2$. This localized region of high pressure moves liquid away from the spot and creates a vortex pair near the membrane's surface. This event, in turn, causes a thinning of the ESC region. On the other hand, the diffusion in the electroneutral region stabilizes
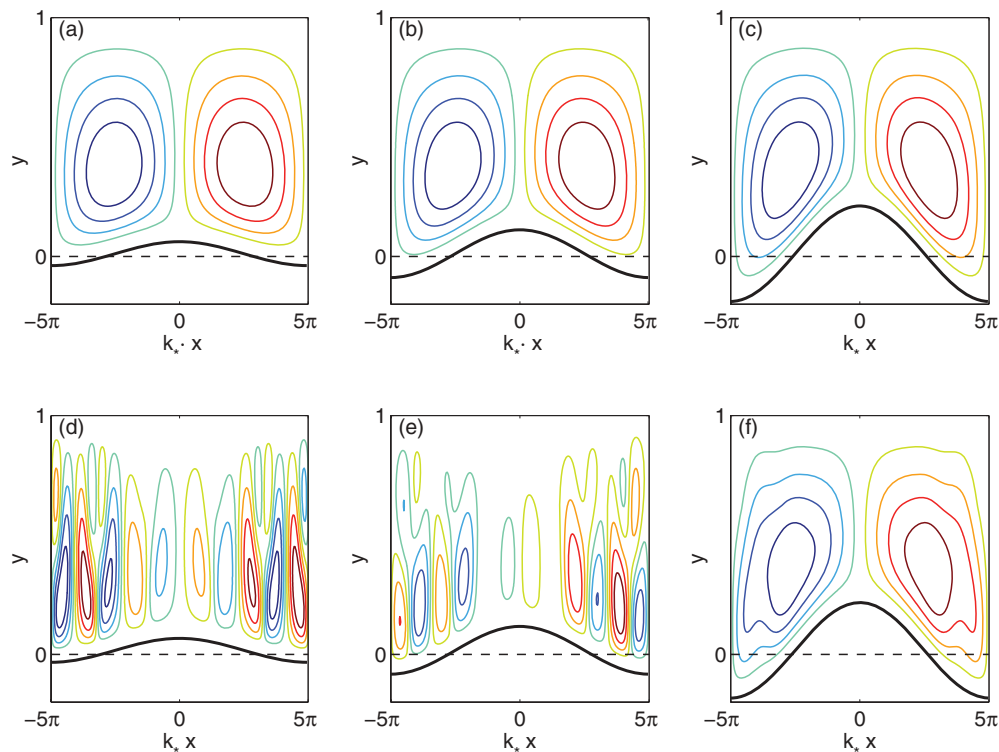


FIG. 3. (Color online) Streamlines of electroconvective vortex pairs for different amplitudes of corrugation: (a), (d) $a = 0.05$, (b), (e) $a = 0.1$, and (c), (f) $a = 0.2$, and for the fixed wave number of corrugation $q/k_* = 0.2$. (a)–(c) correspond to the subcritical case $\Delta V / \Delta V_* = 0.90$, and (d)–(f) correspond to the supercritical case $\Delta V / \Delta V_* = 1.02$.
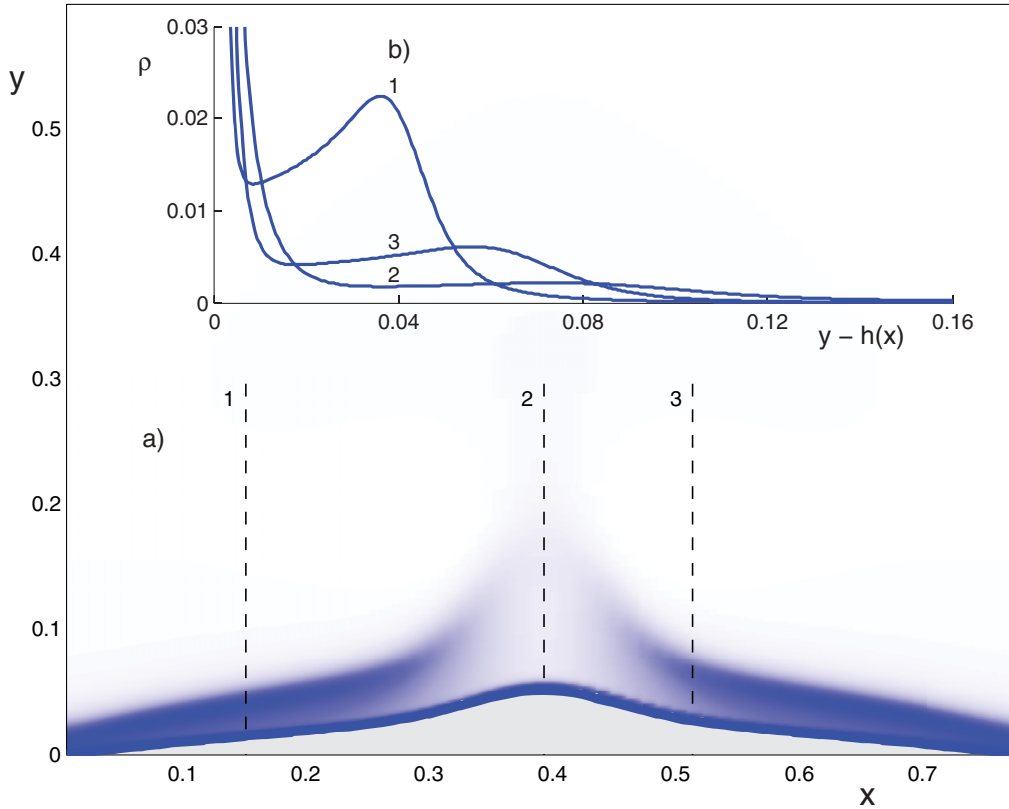
FIG. 4. (Color online) (a) Space charge distribution $\rho(x,y)$ along a curved boundary for the subcritical regime, $\Delta V = 20$ (Dukhin's mechanism of electroconvection). Darker regions correspond to larger charge densities. (b) Charge profiles along the $y$ coordinate for the different cross sections 1, 2, and 3.

the disturbances, which decay for the limiting regimes and grow for the overlimiting ones. This strong mechanism affects the inner structure of the ESC region and manifests itself even for flat surfaces.

The main influence of the curved boundary is expected in the diffusion region. As in Dukhin's electro-osmotic phenomenon of the second kind (see [1,11,12]), screening of the normal field changes the extended polarized region along the curved surface and produces a varying normal field along the surface. This variation creates electro-osmotic velocity near the curved surface, and an inhomogeneity of that velocity along the membrane produces electroconvective vortices. Note that the inner structure of the ESC layer [11] is untouched by the curved boundary.

The physical mechanisms of both modes of electroconvection are very different, thus their interaction is expected to be nontrivial.

The transition from the limiting regimes to the overlimiting ones can be caused, in particular, by electrokinetic instability, and, in this case, the transition parameters are determined by the critical values of the threshold of this instability. (Regarding other mechanisms of the transition to the overlimiting currents, see [3,13,14].) The marginal stability curve was calculated numerically, considering sinusoidal perturbations in the $x$ direction and expanding the eigenfunctions in Chebyshev polynomials in the $y$ direction, eventually solving the resulting matrix eigenvalue problem by the QR algorithm. The linear stability results were tested by using another method [15]

and are presented in Fig. 2 using the critical parameters $\Delta V_* = 29.5$ and $k_* = 4.63$, which separate the limiting and overlimiting regimes. The potential drop and the wave number will be referred to these values.

*Subcritical regimes*, $\Delta V < \Delta V_*$. At the flat membrane's surface $a = 0$, for the subcritical case (limiting regimes), the solution is one dimensional and uniform along the membrane, $\partial/\partial x = 0$, and, hence, the tangential electric field is absent and there is no hydrodynamic motion. The flux of ions is carried out by diffusion and electromigration. At $a \neq 0$, the uniformity in the $x$ direction is violated and the corrugation creates a tangential field along with hydrodynamic motion, and an additional convective mechanism of current transfer is established.

This enhancement can be qualitatively captured using the same linearized statement as for the stability problem; see the inset of Fig. 2. The amplitude $j_{\max} - j_{\min}$ is in phase with the wall corrugation, i.e., a maximum of $h(x)$ corresponds to a maximum of the current amplitude, and vice versa. The linear response to the wavy boundary was calculated from the linearized system of equations; this response is finite outside of the criticality and has a maximum at $q = k_*$. The amplitude of this maximum becomes infinitely large as $\Delta V/\Delta V_* \to 1$. For $\Delta V > \Delta V_*$, the linear approach is not applicable.

The restrictions of the linear theory can be removed by simulation of the full nonlinear system (3)–(11). The typical calculations are illustrated in Figs. 3(a)–3(c), where the streamlines of the electroconvective flow are presented for different amplitudes of corrugation $a$ and a fixed wave number $q$.
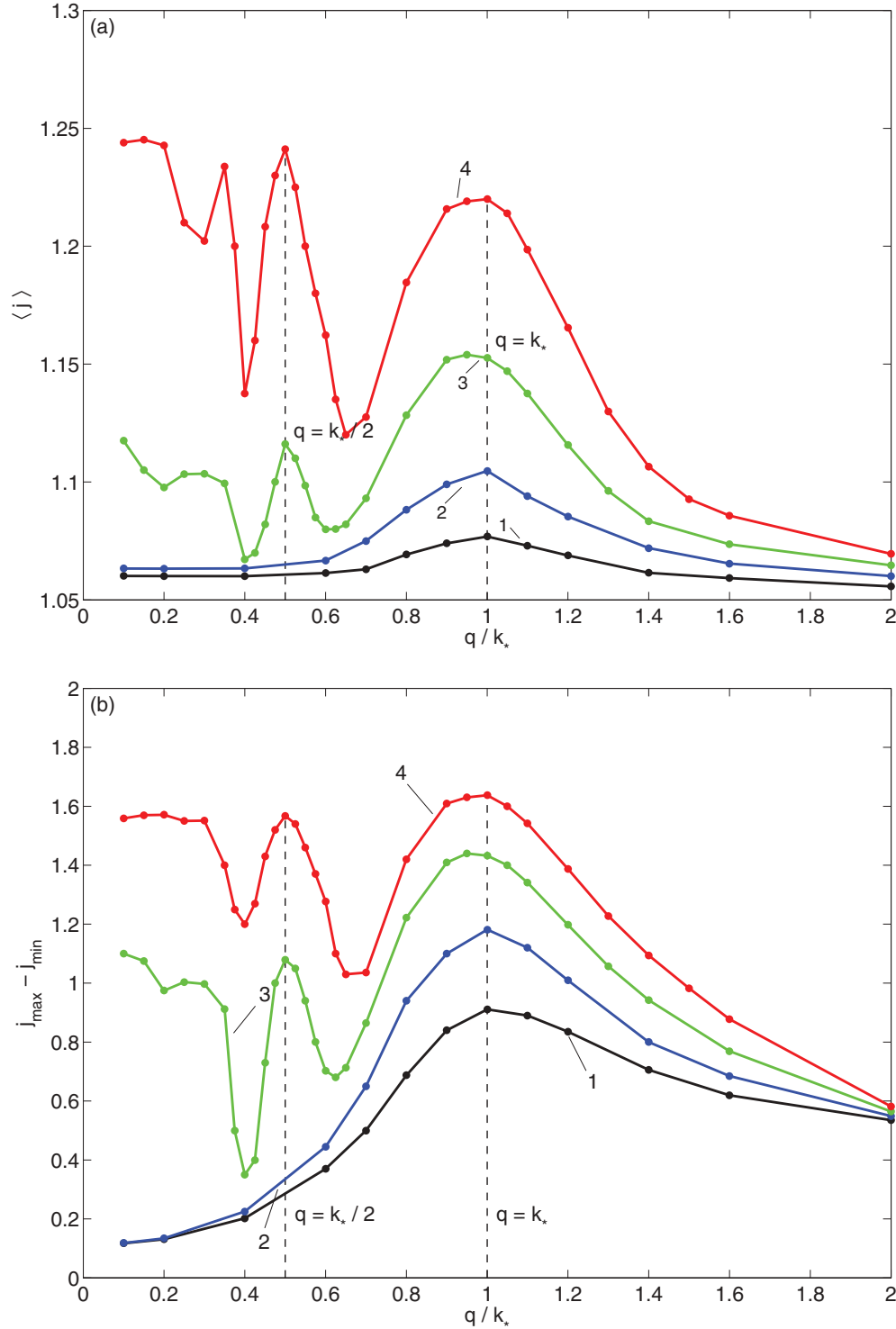
FIG. 5. (Color online) (a) Average electric current $\langle j \rangle$ and (b) current amplitude $j_{max} - j_{min}$ vs normalized wave number of corrugation $q/k_*$ and different $\Delta V/\Delta V_*$: $\Delta V/\Delta V_* =$ (1) 0.90, (2) 0.96, (3) 1.02, and (4) 1.08, for the fixed amplitude of corrugation $a = 0.05$.

The dependence of the average electric current $\langle j \rangle$ and current amplitude $j_{max} - j_{min}$ on the wave number $q$ at a fixed amplitude $a = 0.05$ shows the maximum of flux when the wave number of corrugation coincides with the critical wave number of electrokinetic instability, $q = k_*$, which is in qualitative accordance with the prediction of the linear theory (see Fig. 5, lines 1 and 2). Moreover, for small

amplitudes, $a < 0.005$, and reasonably far from the critical point, the linear analysis is in quantitative agreement with the nonlinear numerical simulations. The maximum becomes more pronounced at the critical potential drop, $\Delta V = \Delta V_*$ (Fig. 5, line 3); unlike the linear theory, this maximum is finite. The dependence of $\langle j \rangle$ on the amplitude $a$ for the limiting regimes is monotonic; see Fig. 6, lines 1 and 2. The dash-dotted
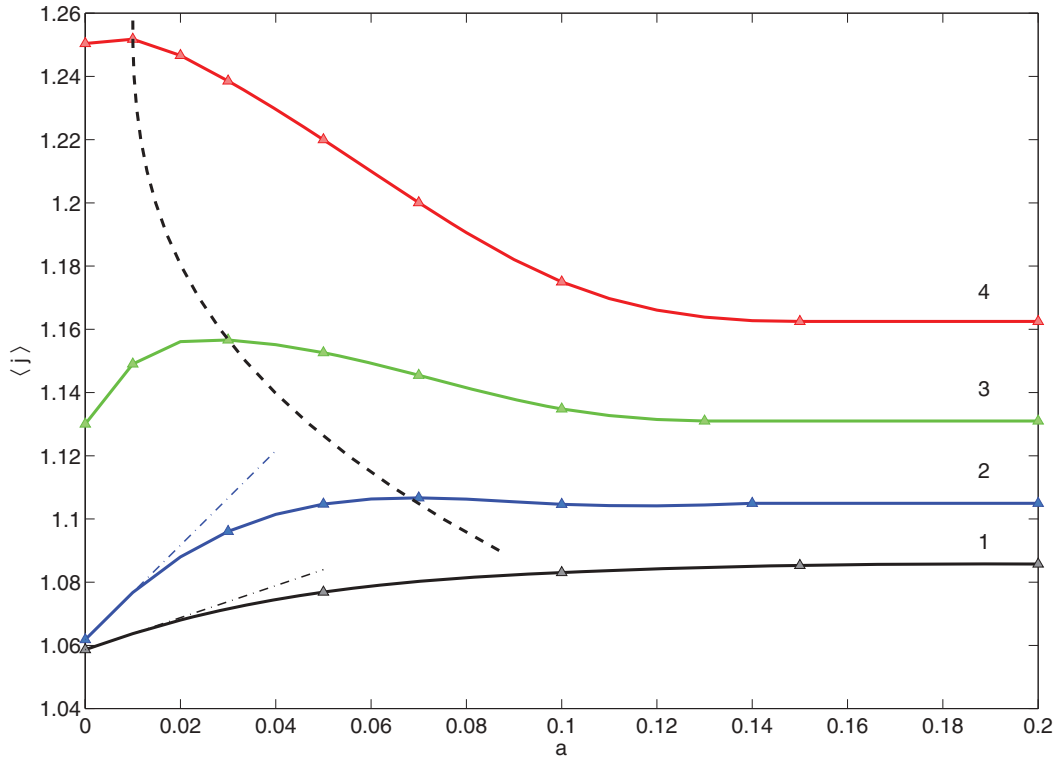
FIG. 6. (Color online) Averaged current $\langle j \rangle$ vs corrugation amplitude $a$ for $q = k_*$ and different $\Delta V / \Delta V_*$: (1) 0.90, (2) 0.96, (3) 1.02, and (4) 1.08. The dashed line stands for maxima of $\langle j \rangle$. Dash-dotted lines corresponds to the prediction of the linear theory.

straight line is the response predicted by the linear theory. The limitation of the linear theory with very small amplitudes can be seen from the figure. For large $a$, there is a saturation of the current on amplitude.

The space charge distribution has a sharp boundary with a diffusion region, $O(\nu^{2/3})$ (see [5]). This boundary for the wavy membrane and large enough amplitude of corrugation has a spikelike profile with a cusped apex (see Fig. 4), where $h = 0.05 \exp\left[-15\left(x - \frac{\pi}{8}\right)^{3/2}\right]$. The angle of the cusped apex can be approximately determined; it practically does not depend on the problem parameters and is about $100°$ with accuracy $\pm 10°$. (For a small amplitude of corrugation, this boundary remains smooth and no cusped apex is present.)

*Supercritical regimes,* $\Delta V > \Delta V_*$. Even at $a = 0$, the mentioned one-dimensional solution, uniform along the membrane, is unstable. This instability causes electroconvection which sustains a tangential electric field and, thereafter, a hydrodynamic liquid flow. If $a \neq 0$, that is, if two mechanisms of the electroconvective flow are involved, then the behavior for the overlimiting regimes becomes much more sophisticated.

Such an interaction between the instability and the wall corrugation is a well-known phenomenon for other hydrodynamic flows. While the inset of Fig. 1 suggests that the two mechanisms interact resonantly to produce the maximum vortex intensity and ion current when the wave number $q$ of the curved surface coincides with the critical wave number $k_*$ of the instability, classical nonlinear dynamics theory suggests that resonant positive interaction can still occur at other wave number ratios with local current and vorticity maxima or, more interestingly, minima, because of a negative resonant

interaction. In particular, one expects subharmonic resonance at $q/k_* = 1/2$ and, perhaps, when the ratio is a rational number. We will explore these resonant structures numerically by varying the corrugation amplitude and wave number. For a liquid film falling on an inclined plane at small Reynolds numbers, the corrugation suppresses the surface instability [16]. For large Reynolds numbers, this interaction becomes more complicated [17] and can both stabilize and destabilize the flow. The Tollmien-Schlichting instability in the boundary layer can either be suppressed or intensified by wall corrugation, depending on its parameters [18]. For river shock waves, the interaction between the topography of the river's bottom and the surface instability can completely change the flow regime [19].

Both electroconvective modes can weaken or amplify each other. The streamlines of the flow for different amplitudes $a$ and a fixed wave number $q$ for the overlimiting regimes are presented in Figs. 3(d)–3(f). They are very different from those presented in the same figure for the limiting regimes presented in Figs. 3(a)–3(c). For a small amplitude $a = 0.05$ and a long enough corrugation, there is mainly a manifestation of the electrokinetic instability, but unlike the flat channel case, the vortices of the electrokinetic instability are distorted by the corrugation. One sees in Fig. 6 that for $q = k_*$ (1 : 1 resonance), the interaction is increasingly negative at larger overcritical conditions, i.e., with increasing amplitude $a$, the average current $\langle j \rangle$ is decreasing.

The vortex distribution along the curved surface at different wave numbers $q$ and at a fixed amplitude $a$ is shown in Fig. 7. For small $q$, the behavior is unsteady and irregular, but
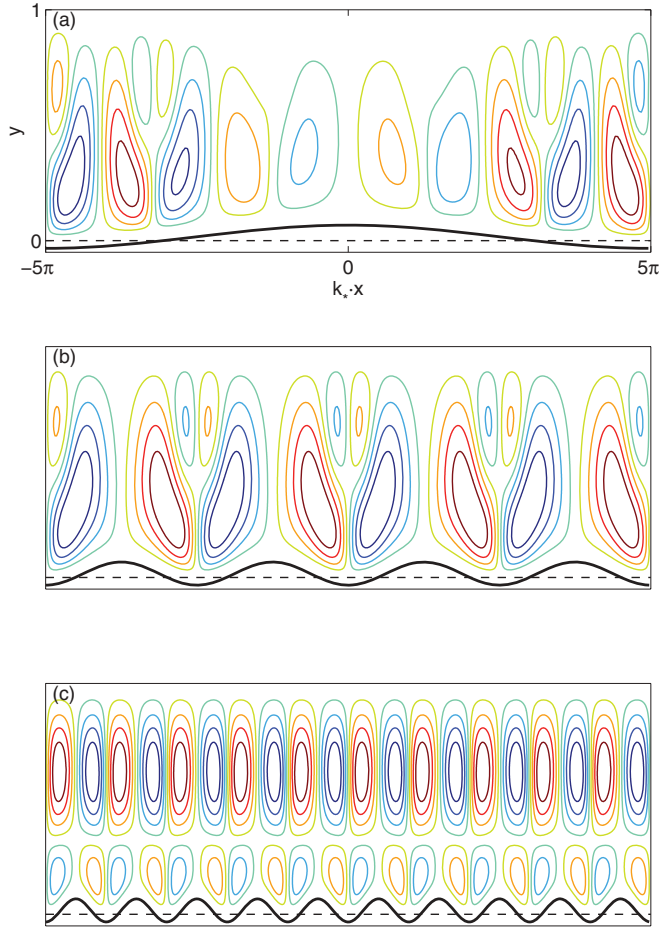
FIG. 7. (Color online) Streamlines of vortex pairs for different wave numbers of corrugation: $q/k_* = $ (a) 0.1, (b) 0.8, and (c) 2.0, and the fixed amplitude $a = 0.05$ for the overlimiting case $\Delta V/\Delta V_* = 1.02$.
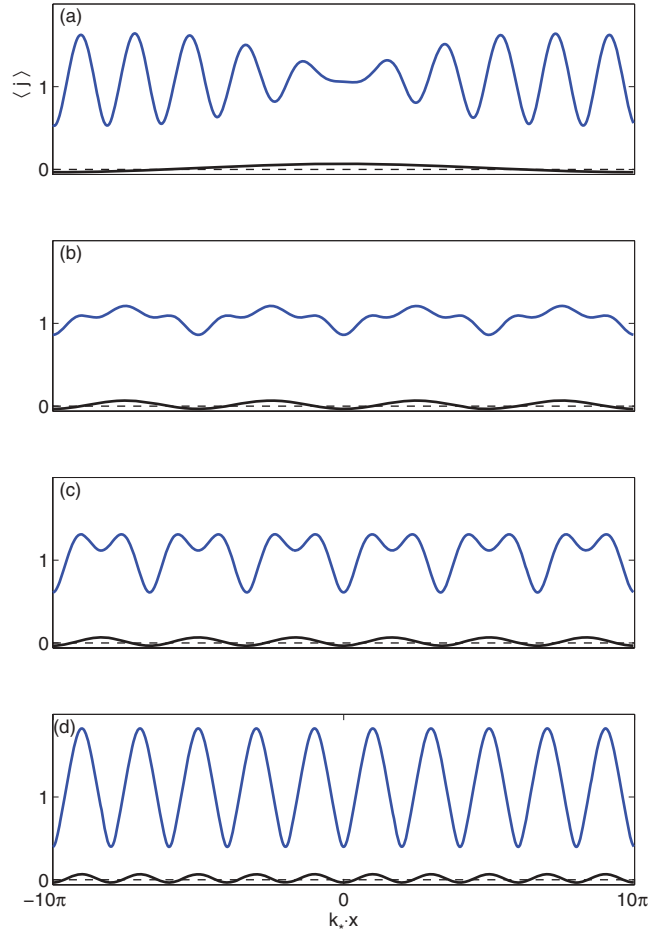


FIG. 8. (Color online) Electric current distribution along the membrane, $j(x)$, for different wave numbers of corrugation $q$ and a fixed amplitude $a = 0.05$: $q/k_* = $ (a) 0.1, (b) 0.4, (c) 0.6, and (d) 0.8. Overlimiting regime, $\Delta V/\Delta V_* = 1.02$.

approaching the instability's asymptote at vanishing amplitude and finite overcritical voltage. The corresponding snapshot is presented in Fig. 7(a). With increasing wave number of corrugation, the picture becomes steady and regular; the instability and corrugation balance each other [see Fig. 7(b)]. In Fig. 7(c), for sufficiently large $q$, the electrokinetic instability eventually succumbs to the corrugation. For larger $q$, the behavior does not change and the corrugation suppresses the instability.

The behavior at intermediate wave numbers $q$ is worth more discussion. The electric current distribution along the membrane is shown in Fig. 8. At small $q$ [Fig. 8(a)], the corrugation creates an envelope in the current distribution, much like Floquet instability for periodic waves; see, for example, [20]. With increasing $q$ [Fig. 8(b)], the two modes of electroconvection balance each other and the resulting current amplitude $j_{\max} - j_{\min}$ is very small. With further increase of the wave number, the corrugation's mode prevails over the instability's mode, and the reaction of the flow to the corrugation is sinusoidal.

The dependence of the average electric current $\langle j \rangle$ on the wave number $q$ at a fixed amplitude $a$ complements the description (see Fig. 5, lines 3 and 4). For very small $q$, $q/k_* < 0.1$, the averaged current is not sensitive to the corrugation and is determined entirely by the instability. With increasing wave

number, the corrugation suppresses the instability, achieving minima at $q/k_* \approx 0.3$ and $q/k_* \approx 0.4$. It is surprising that with a further increase of $q$, the average current $\langle j \rangle$ shows a maximum when the wave number of corrugation coincides with either the critical wave number of the electrokinetic instability $k_*$ or its subharmonic $\frac{1}{2}k_*$. At these points, the corrugation becomes more efficient for ion transfer and both modes strengthen each other. If the maximum at $q = k_*$ stems from the one for the limiting regimes (see Fig. 5, lines 1 and 2), then the maximum at the subharmonic wave number arises only for the overlimiting regimes. Summarizing, one can say that "sideband corrugation" weakens instability, while subharmonic corrugation amplifies it. A further increasing in $q$, $q > k_*$, leads to the dominance of the curvature-induced Dukhin's vortices over the instability.

The dependence on amplitude for the overlimiting regimes is not monotonic; it also has a maximum for some amplitude. With increasing $\Delta V/\Delta V_*$, this maximum is shifted to smaller amplitudes; see Fig. 6, lines 3 and 4.

The general trend of this paper has been to investigate the combined effect of two modes of electroconvection: the electro-osmotic flow of the second kind induced by the membrane surface's curvature (Dukhin's mechanism) and the

electrokinetic instability (Rubinstein-Zaltzman's mechanism). It was found that both modes can suppress or intensify each other. Depending on the system parameters, some particular parts of the channel can contain vortices and some can be stable. This phenomenon can be used in micro- and nanochannels with nonuniform surfaces.

[1] S. S. Dukhin, Adv. Colloid Interface Sci. **35**, 173 (1991).

[2] I. Rubinstein and B. Zaltzman, Phys. Rev. E **62**, 2238 (2000).

[3] Y. K. Suh, Phys. Rev. E **85**, 036305 (2012).

[4] I. Rubinstein and B. Zaltzman, Phys. Rev. E **68**, 032501 (2003).

[5] B. Zaltzman and I. Rubinstein, J. Fluid Mech. **579**, 173 (2007).

[6] D. Goldstein, R. Handler, and L. Sirovich, J. Comput. Phys. **105**, 354 (1993).

[7] N. Nikitin and A. Yakhot, J. Fluid Mech. **532**, 141 (2005).

[8] A. Yakhot, L. Grinberg, and N. Nikitin, J. Biomech. **38**, 1115 (2005).

[9] E. A. Demekhin, V. S. Shelistov, and S. V. Polyanskikh, Phys. Rev. E **84**, 036318 (2011).

[10] C. Canuto, M. Hussaini, A. Quarteroni, and T. Zang, *Spectral Methods in Fluid Dynamics* (Springer-Verlag, Berlin, 1987).

[11] Y. Ben and H.-C. Chang, J. Fluid Mech. **461**, 229 (2002).

[12] Y. Ben, E. A. Demekhin, and H.-C. Chang, J. Colloid. Interface Sci. **276**, 483 (2004).

[13] I. Rubinstein and L. Shtilman, J. Chem. Soc., Faraday Trans. 2 **75**, 231 (1979).

[14] I. Rubinstein and B. Zaltzman, Math. Models Methods Appl. Sci. **11**, 263 (2001).

[15] E. Demekhin, E. Shapar, and V. Lapchenko, Dokl. Phys. **53**, 450 (2008).

[16] Yu. Ya. Trifonov, J. Appl. Mech. Tech. Phys. **45**, 3, 389 (2004).

[17] A. Wierschem, T. Pollak, C. Heining and N. Aksel, Phys. Fluids **22**, 113603 (2010).

[18] D. N. Riahi, J. Fluid Dyn. Res. **25**, 3 129 (1999).

[19] E. Demekhin, E. Shapar and A. Selin, Thermophys. Aeromech. **15**, 2, 243 (2008).

[20] H.-C. Chang and E. A. Demekhin *Complex Wave Dynamics on Thin Films* (Elsevier, Amsterdam, 2002).